Asian Journal of Chemistry; Vol. 37, No. 10 (2025), 2545-2551
ASIAN JOURNAL OF CHEMISTRY
https://doi.org/10.14233/ajchem.2025.34351

Synthesis of Nanocomposite Materials Based on TiO_2 Nanotubes and Polymethylene Naphthylene Sulfonate and their Electrophysical Properties

JAKHONGIR KARSHIBAYEV[1,], SHERZOD DJUMAGULOV[2,*,], OLIM RUZIMURODOV[3,], DOSTON NURMATOV[4,], TOLMAS MANSUROV[5,], SULTAN AKHMEDOV[6,], VAZIRA OTAKUZIYEVA[6,] and NILUFAR ASKAROVA[7,]

[1]Department of Biology, Gulistan State University, Syr Darya, 120100, Uzbekistan
[2]Department of Organic and Petroleum Chemistry, National University of Uzbekistan named after Mirzo Ulugbek, Tashkent, 100174, Uzbekistan
[3]Department of Natural and Mathematical Sciences, Turin Polytechnic University in Tashkent, Tashkent, 100095, Uzbekistan
[4]Department of Chemistry, Chirchik State Pedagogical University, Chirchik, 111718, Uzbekistan
[5]Department of Chemical Technology, Yangiyer branch of Tashkent Chemical Technology Institute, Yangiyer, 121000, Uzbekistan
[6]Department of Chemical Engineering and Geodesy, Kokan Branch of Tashkent State Technical University named after Islam Karimov, Fergana, 100095, Uzbekistan
[7]Department of Metallurgy, Almalyk Branch of Tashkent State Technical University named after Islam Karimov, Almalyk, 100000, Uzbekistan

*Corresponding author: Fax: +998 88 9080293; Tel: +998 94 6327277; E-mail: asadbekkambaraliev161@gmail.com

Received: 27 June 2025 *Accepted*: 22 September 2025 *Published online*: 30 September 2025 AJC-22139

In this study, nanocomposite materials composed of titanium dioxide (TiO_2) nanotubes and polymethylene naphthylene sulfonate (PMNS) were successfully synthesized and extensively characterized. TiO_2 nanotubes were fabricated *via* electrochemical anodization in an ethylene glycol-based electrolyte containing ammonium fluoride, under varying voltage and time conditions. Scanning electron microscopy (SEM) and Fourier-transform infrared spectroscopy (FTIR) analyses confirmed the formation of well-aligned, porous nanotube structures with diverse lengths and morphologies. A detailed investigation was carried out to evaluate the influence of anodization voltage (ranging from 20 to 80 V) and electrolyte composition on the height and surface uniformity of the nanotubes. PMNS was synthesized through the sulfonation and subsequent polycondensation of β-naphthalene sulfonic acid with formaldehyde under precisely controlled thermal and stoichiometric conditions. The structural characteristics of the resulting polymer were examined using IR spectroscopy, complemented by quantum chemical calculations, including HOMO-LUMO energy gap analysis and charge distribution profiling. The TiO_2 nanotubes were then combined with PMNS through an electrochemical polymerization technique to create the final nanocomposites. Their electrochemical behaviour was studied using voltammetric techniques, revealing that both the electrolyte composition and nanotube architecture significantly affect the electrical conductivity. These composites exhibited distinctive p-type and n-type semiconducting behavior, which is strongly influenced by the polymer/oxide interface. Overall, the TiO_2-PMNS nanocomposites demonstrated promising electrical performance, suggesting their potential application in smart electrochemical devices, supercapacitors, and sensor technologies. This work contributes to the development of advanced nanomaterials based on semiconducting polymers and provides valuable insights into the structure-property relationships critical for next-generation electronic systems.

Keywords: Anodization, Pore formation kinetics, Voltammetric and Amperometric properties.

INTRODUCTION

Electrochemical synthesis and anodization techniques have garnered more interest in the past ten years [1-3]. Since the nanomaterials made from porous anodic oxides [4], like porous aluminum and titanium nanotubes [5], have enormous potential in a variety of fields [6], particularly anode side of TiO_2 nanotubes (ATO) for conversion of solar energy, photocatalytic decomposition sensors supercapacitors and solar energy conversion to hydrogen fuel [7-10], they have garnered a lot of scientific attention. Numerous factors, such as electrolyte concentration, anode voltage, current density and electrolyte temperature, influence the formation of pores and nanotubes [11, 12]. For instance, different works of literature have varying measurements for the height of nanotubes [13-15].

According to previous studies [16,17], significant differences have been observed in the elevation of nanotubes synthesized using ethylene glycol-based electrolytes with a con-

sistent ammonium fluoride concentration (0.3% NH_4F). For instance, anodization carried out at a current density of 10 $mA \cdot cm^{-2}$ for 45 min resulted in nanotubes with a height of 15.3 μm, whereas a lower current density of 7.5 $mA \cdot cm^{-2}$ produced nanotubes measuring only 4.7 μm in height [18,19]. Moreover, anodization at a constant voltage of 50 V for 60 min yielded nanotubes with a height of approximately 8.5 μm [20].

The influence of the titanium substrate on the growth and dimensions of nanotubes was also examined using an electrolyte containing 0.3% NH_4F. Nanotubes formed under a constant anodizing voltage of 60 V for 360 minutes exhibited heights ranging from 32 to 50 μm [21-24]. These results highlight that nanotube height is significantly influenced by the multiple parameters including anodizing current, substrate type, applied voltage and anodizing duration even within the same NH_4F-based electrolyte. This indicates that the nanotube height is not solely governed by the electrochemical dissolution reaction involving fluoride ions ($TiO_2 + 6F^- + 4H^+ \rightarrow [TiF_6]^{2-} + 2H_2O$) [25,26].

For example, nanotubes with a height of 29.8 μm were synthesized using an ethylene glycol electrolyte containing 0.3% NH_4F and 0.2% water at 60 V for 180 min. In contrast, anodization in an electrolyte with 0.5% NH_4F and 2% water at the same voltage for just 10 min resulted in nanotubes with a height of 9.0 μm [27-30]. Furthermore, a height of 10 μm was obtained using an electrolyte with 0.83% NH_4F and 8% water at 60 V for 360 min [31-33]. These variations confirm that water content significantly affects nanotube height, as it alters the dissolution kinetics in conjunction with the fluoride ion concentration [34,35].

The investigation of the kinetics and mechanisms involved in the synthesis of semiconducting polymers [36], along with the development of new compositions and the analysis of their physical, chemical and physico-chemical properties, holds significant scientific relevance in light of the rapid advancement of global electronic technologies [37-40].

EXPERIMENTAL

Strips of 0.1 mm thick titanium foil (10 mm × 40 mm) with 99.8% purity (Sigma Aldrich) were polished. To get rid of roughness and contaminants, the foil surface was cleaned for 15 min using an $HF:HNO_3:H_2O$ (1:1:2) solution (GT Sonic-D 6, 220-240V AC). After 15 more min of washing in distilled water, it was left outside to dry for 1 h. Following that, an electrolyte was made with 0.1 and 0.2% NH_4F, 2% water and 98% ethylene glycol solution.

A graphite electrode served as electrode in the opposite direction, while titanium foil was acted as anode. The titanium foil had a 4 cm^2 surface area when submerged in the electrolyte (2 cm × 1 cm × 2 sides). From 30 V to 70 V, the voltages were applied in various sequences (potentiostat: Model SS-350 M, S/N 21121062). Constant anodizing process voltages were supplied to the two-electrodes in two distinct electrolytes for the purpose of having anodizing periods of 2, 3, 4 and 6 h. Every procedure was carried out three times.

Polycondensation of β-naphthalenesulfonic acid with formaldehyde (35%): The polycondensation process was carried out in a sealed, hermetically closed reactor equipped with a mechanical stirrer to ensure the uniform mixing. β-Naphthalenesulfonic acid and aqueous formaldehyde solution (35%) were combined in a molar ratio of 1:0.8. The reaction mixture was maintained at 90-100 ºC and stirred continuously for 5 h under controlled thermal conditions to promote effective polymer chain formation (**Scheme-I**). As a result of this process, polymethylenenaphthalenesulfonic acid was obtained with a yield of 82.4%, indicating efficient condensation.

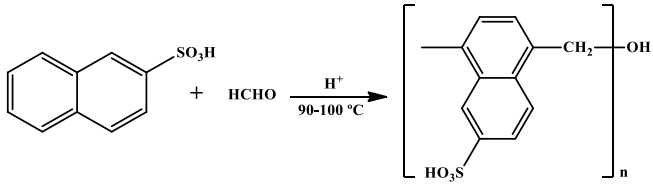

Scheme-I

Synthesis of nanocomposites: Nanocomposites comprising TiO_2 nanotubes and copolymer, polymethylene naphthalene sulfonate were synthesized using an electrochemical polymerization method. In this setup, graphite served as the counter electrode, titanium dioxide (TiO_2) nanotubes acted as the working electrode (anode) and the electrolyte consisted of 15 g of polymer dissolved in 100 g of DMSO. Nanocomposites were synthesized using electrolytes containing varying water contents (45%, 10% and 2%, labeled as samples a, b and c, respectively). The exposed surface area of the TiO_2 nanotubes in the electrolyte was approximately 4 cm^2. Sequential voltages of 50 V and 60 V were applied during the process. Electro-chemical polymerization was carried out over a period of 4 h, with voltage continuously applied across both electrodes in five different electrolyte systems. Each anodization experiment was repeated three times to ensure reproducibility.

RESULTS AND DISCUSSION

The formation of TiO_2 nanotubes from nanoporous structures requires the dissolution of titanium oxofluorides generated between the tube walls. Among the key factors influencing this process is the chemical aggressiveness of the surrounding environment. During nanotube formation, fluoride ions (F^-) in the electrolyte react with Ti^{4+} ions released from the metal surface, forming soluble $[TiF_6]^{2-}$ salt. The presence of fluorine within the nanotubes was confirmed through infrared spectroscopy. The key vibrational bands observed include the –Ti–OH stretching at 3489.54 cm^{-1}, the Ti–O–C stretching at 989.69 cm^{-1} and the O–Ti–O stretching at 750 cm^{-1}, all within the spectral range of 4000–500 cm^{-1}. The presence of –Ti–OH groups in the sample indicates an alkaline medium, as evidenced in Fig. 1a. The Ti–O–C stretching vibration is observed at 989.69 cm^{-1}, while the O–Ti–O stretching vibration appears at 750 cm^{-1}. In contrast, the spectrum in Fig. 1b corresponds to a sample formed in a neutral medium. In another sample (Fig. 1c), the stretching vibration of the C–H group appears at 3121.15 cm^{-1}, Ti–OH at 3489.54 cm^{-1} and O–Ti–O at 750 cm^{-1}. The presence of Ti–OH once again confirms the alkaline nature of the medium.

Morphological studies: The formation of nanotubes is shown in Fig. 2a-b, which shows the development of highly

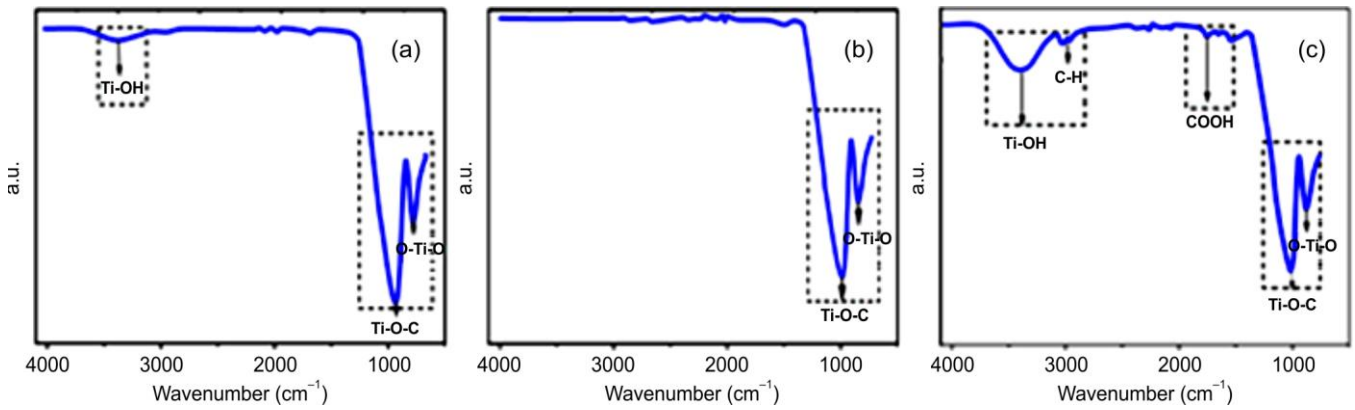

Fig. 1. IR spectra (a-c) of titanium dioxide (TiO_2) nanotubes obtained after anodization

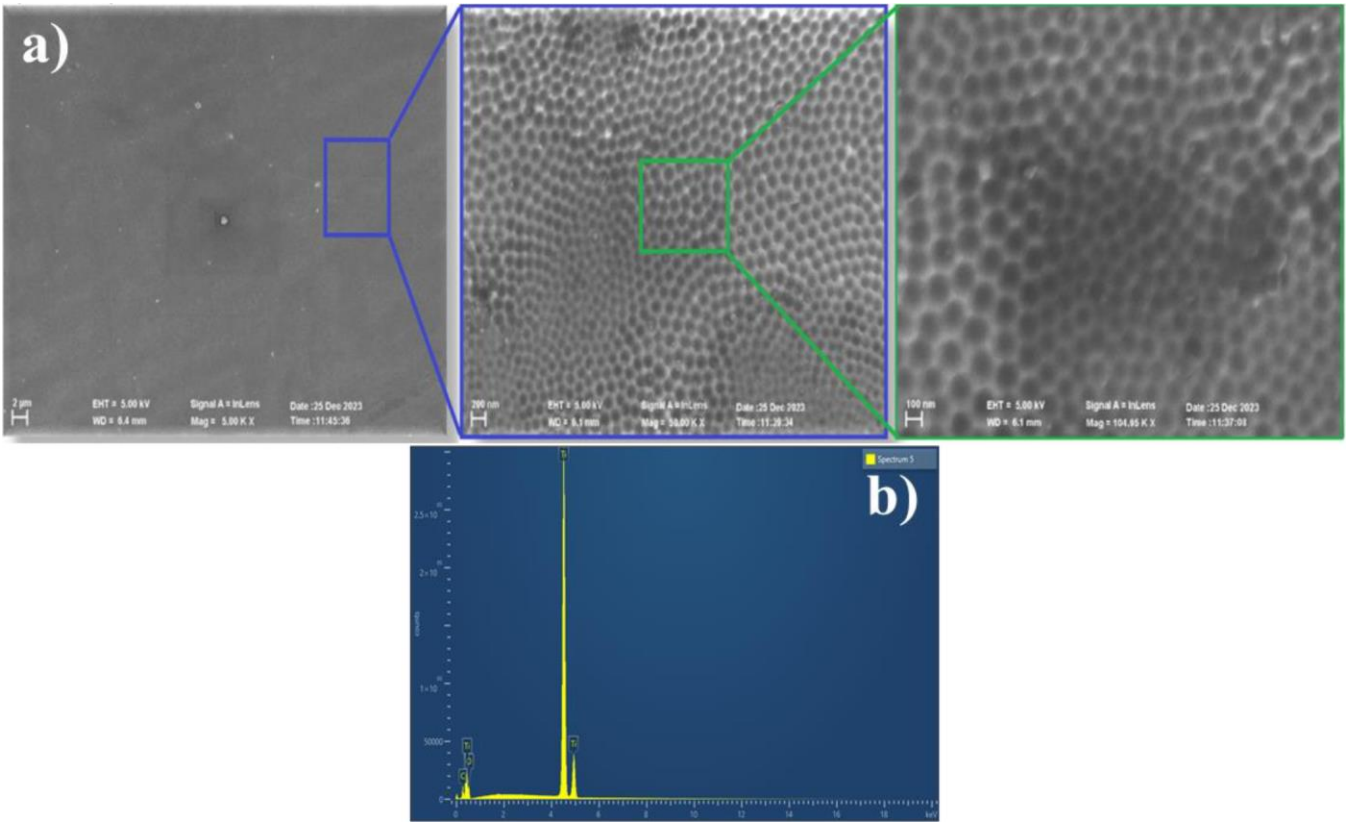

Fig. 2. SEM-EDS (a-b) micrographs of nanotubes obtained at 20 ºC, 60 V with 0.2% NH_4F

ordered, uniform double-layered nanotubes with smooth, flat surfaces. Elemental analysis reveals a composition of 65.55% titanium (Ti), 31.5% oxygen (O) and 3% carbon (C).

In this study, nanotubes were fabricated using a potentiostat at various applied voltages ranging from 20 to 80 V. The oxidation and reduction behaviour of fluoride and oxygen anions in the electrolyte solution is illustrated in Fig. 3a. The current–time curve reveals that at 20 V, the oxidation process began at 57 mA after 5 sec and produced an analytical signal at 36.8 mA after 8.7 sec, indicating the onset of pore transformation into nanotubes. During a 300 sec anodization, the current ranged between 0–65 mA. Following the formation of an oxide layer at 49.7 mA after 18 sec, the process was repeated under similar current density conditions. At 40 V, the oxidation initiated at 42.4 mA after 4 sec and generated an analytical signal at 31.2 mA at 9.1 sec. The oxidation ceased at 45.3 mA after 25.9 sec, with the current density stabilizing. This confirmed the formation of an oxide layer, as the final oxidation current was lower than the initial value.

At 60 V, oxidation started at 32.7 mA and lasted 4 sec. An analytical signal was recorded at 24.6 mA after 5.6 sec and the process concluded at 45.3 mA after 52.9 sec. Again, the development of the oxide layer was indicated by the final current being higher than the starting current. At 80 V, oxidation began at 25.3 mA at 2.8 sec and the analytical signal appeared at 17.6 mA at 2.6 sec. The current density then stabilized as the oxidation process ended at 41.3 mA after 98.9 sec.

The formation of highly ordered nanotubes is indicated when the oxide layer formation current exceeds the initial set current. Although higher voltages such as 100 V, 120 V and

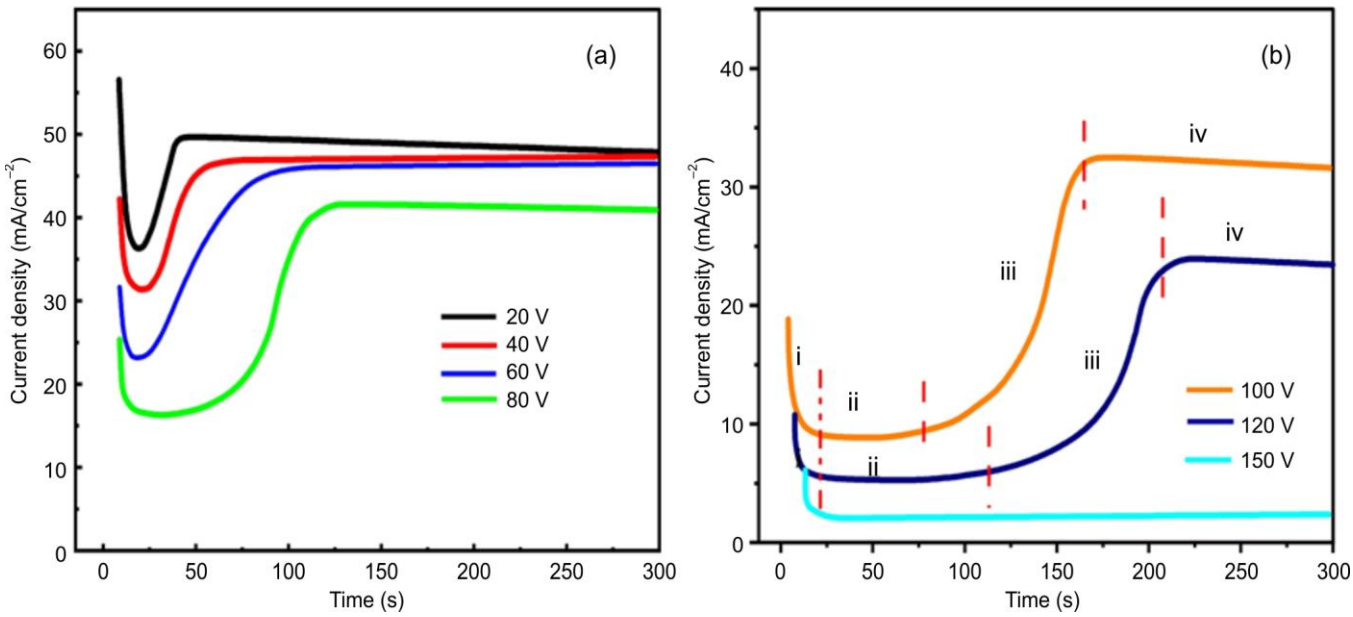

Fig. 3. Time-dependent volt-ampere characteristics of current at (a) voltage (20-80 V) and (b) 1% H_2O (100-150 V)

150 V also resulted in significant oxide layer formation, the resulting nanotubes were irregular and lacked smoothness. This is evidenced by the fact that the oxidation current exceeded the initial current, while the oxide layers formed were disordered (Fig. 1a).

Copolymer: The synthesis of the polymethylene naphthylene sulfonate copolymer follows a single-step process (**Scheme-I**). Under the optimal conditions, with a naphthalene -to-sulfuric acid molar ratio of 1:1.08 and an incubation period of 6 h at 160 ºC, a yield of 82.4% for 2-naphthalene-sulfonic acid was achieved. However, extending the reaction time leads to a reduction in yield due to the occurrence of the secondary side reactions that degrade the desired sulfonic acid products. Infrared spectral analysis of the copolymer revealed characteristic absorption bands: C–H group vibrations at 3061.54 cm^{-1}, C=C stretching at 1596.59 cm^{-1}, –SO_3H group at 1106.18 cm^{-1} and C=O stretching at 1190.57 cm^{-1}.

The morphology, surface texture, and elemental composition of the spatially organized polymethylene naphthalene sulfonic acid were thoroughly examined using SEM, as shown in Fig. 4. Specifically, Fig. 4(c-d) presents high-resolution images that highlight the surface architecture and structural integrity of the synthesized polymer.

DFT computations: To ascertain the route of the aforementioned chemical processes, the Gaussian 09 W software through B3LYP/6-311G*(d,p) program was utilized to investigate the outcomes of quantum chemical computations [41]. The naphthalene molecule's charge distribution, bond lengths, HOMO, LUMO and electrostatic charge distribution values were first determined. Upon examining these quantum chemical calculations, we observe a redistribution of charge in the active sulfo group of the naphthalene molecule (Fig. 5). Here, it can also be seen that the active sulfonic groups in the disulfonaphthalene molecule have excess electrons distributed and react through this active group (Fig. 6).

Physico-chemical characteristics of TiO_2 based nanocomposites: In the IR spectra of TiO_2 nanotubes and TiO_2/polymethylene naphthalene sulfonate (PMNS) nanocomposites, the characteristic peaks corresponding to Ti–O, Ti–OH and –SO_3H groups were clearly observed in both materials. The emergence of new vibrational bands in the range of 1106-989 cm^{-1} upon the incorporation of PMNS confirms the successful formation of the nanocomposite. This also indicates the development of a strong interfacial interaction between the organic polymer (PMNS) and the inorganic TiO_2 matrix.

Water content in the electrolyte was found to significantly influence both the morphology and electrical conductivity of the nanotubes. As the water content of the nanotubes increases, it is evident that irregular, short-diameter states emerge, but the conductivity stays high (0-1.5 V) (Fig. 7a-b). This is mostly due to the current's vertical flow direction, which causes short, wide-diameter nanotubes to develop. Both long and short-diameter nanotubes exhibit low conductivity in the absence of sufficient water. For instance, at 45% water content, rapid dissolution occurred, resulting in nanotubes with large diameters, though they were irregular and uneven in structure. In 10% water, conductivity and stability were in balance, which was considered the optimal result. In 2% water, the nanotubes are long, but conductivity was lower because ion-exchange was slowed down.

Conclusion

This study successfully demonstrated the synthesis and characterization of TiO_2 nanotube-based nanocomposites incorporating polymethylene naphthalene sulfonate (PMNS). TiO_2 nanotubes were fabricated through controlled electrochemical anodization, with their morphology significantly influenced by anodization voltage, time and electrolyte composition. The polymer PMNS was efficiently synthesized and structurally confirmed through FTIR and supported by DFT calculations, highlighting its active sulfonic functional groups. Electrochemical polymerization enabled the integration of PMNS with TiO_2, forming nanocomposites with enhanced electrical behaviour. The interfacial bonding between the oxide

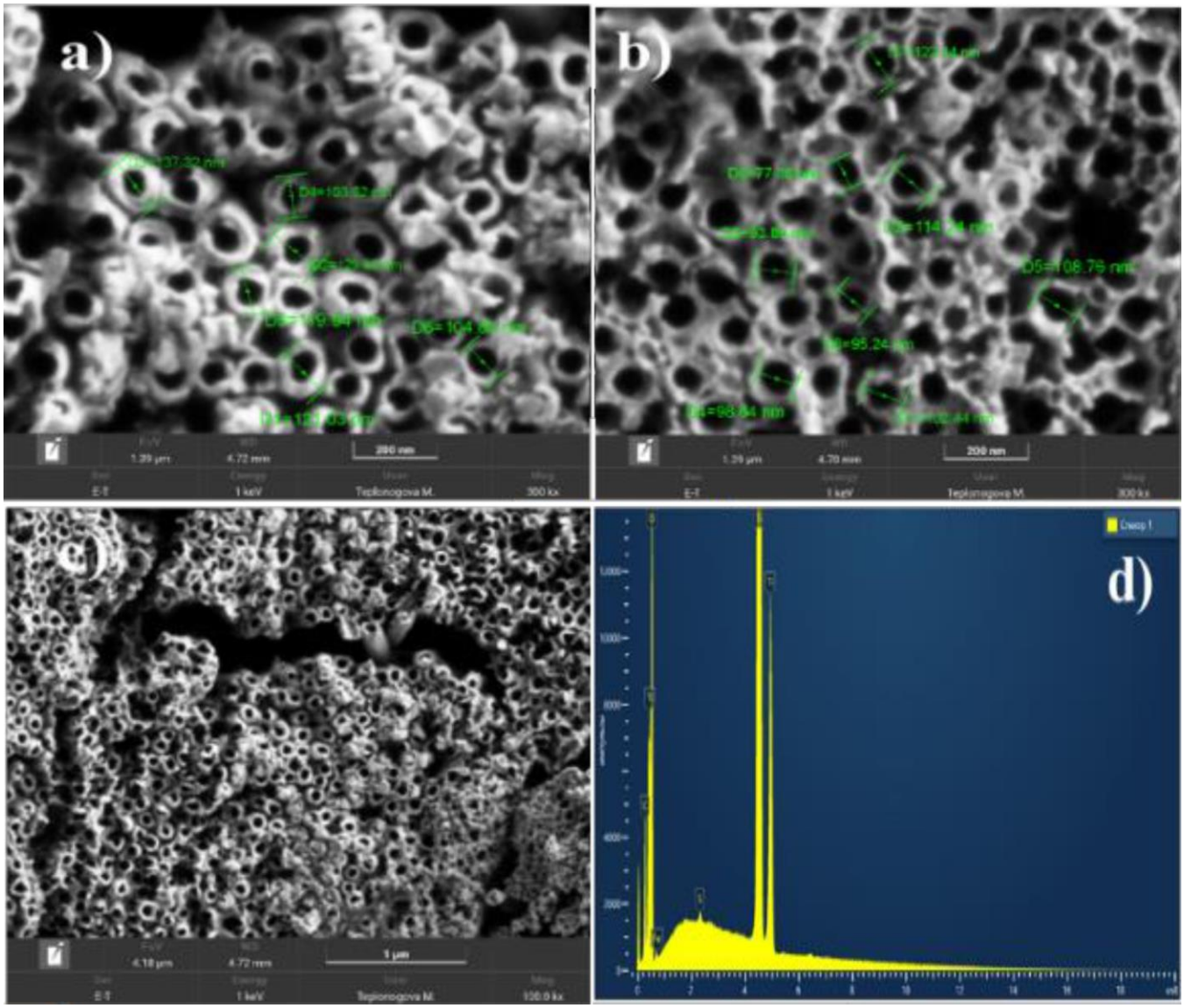

Fig. 4. SEM images of titanium dioxide nanotubes (TiO_2) and TiO_2/PMNS (polymethylene naphthalene sulfonate) nanocomposites

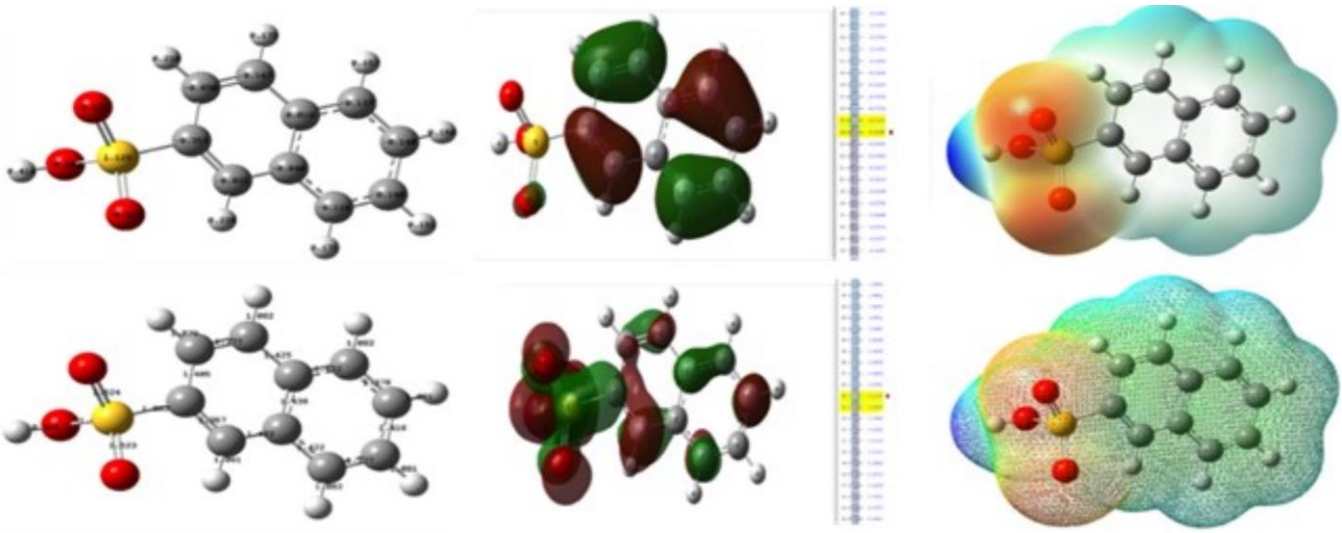

HOMO, LUMO values and Electrostatic charge distribution

Fig. 5. Distribution of charge and bond lengths of the sulfonaphthalene molecule

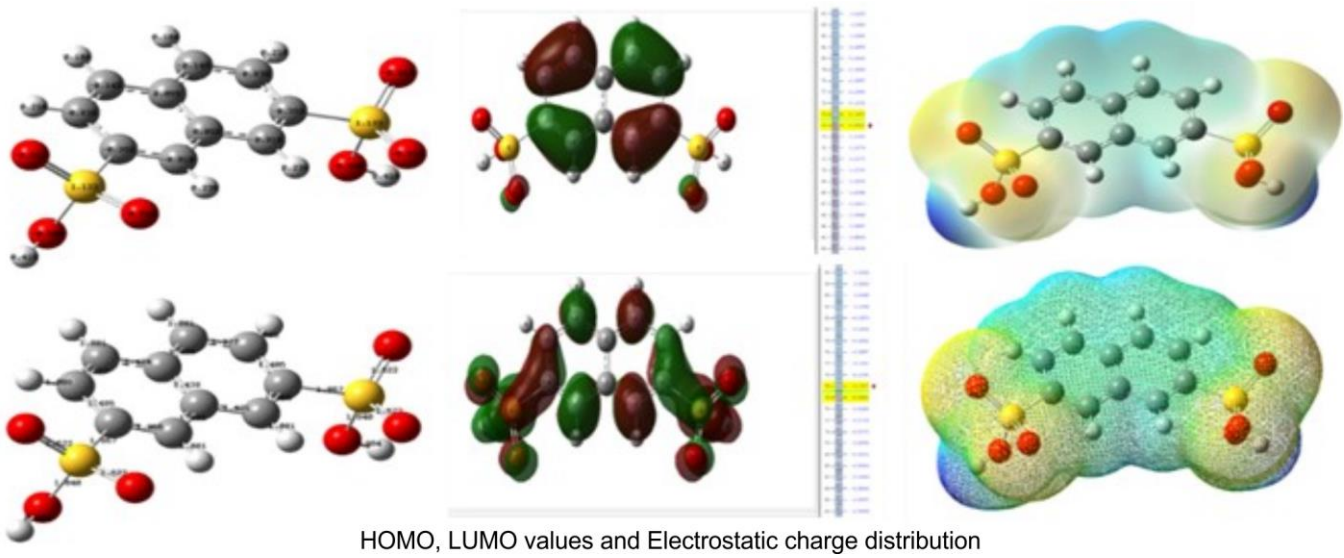

Fig. 6. Distribution of charge, bond lengths of the disulfonaphthalene molecule

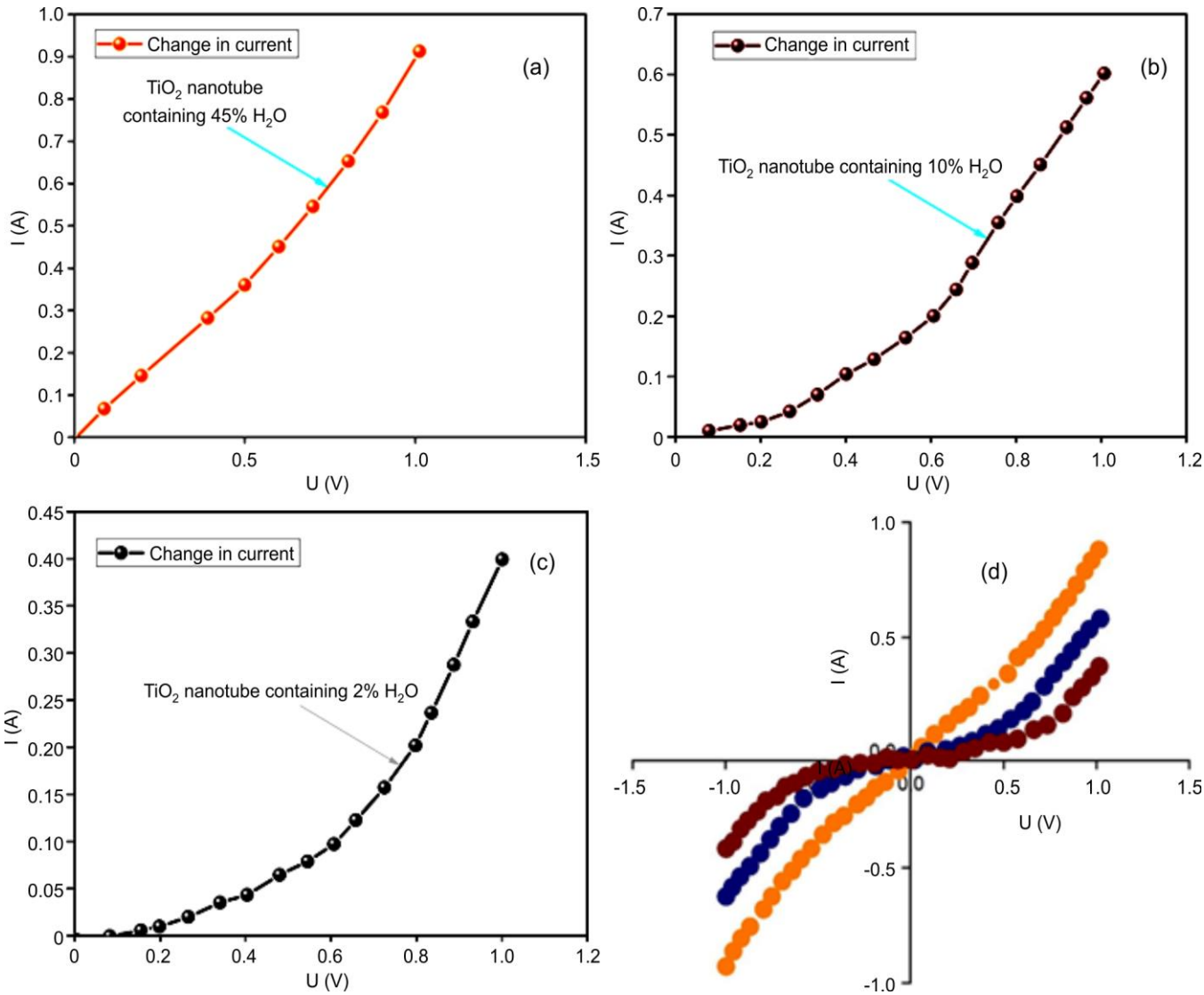

Fig. 7. Voltammetric characteristics of the obtained nanotubes (electrolyte containing 45%, 10% and 2% water (a, b, c)) and their forward and reverse connections

and polymer matrix was evidenced by distinct IR spectral features. Water content in the ethylene glycol-based electrolyte containing ammonium fluoride also played a critical role in tuning both the nanotube morphology and conductivity. Overall, the TiO_2-PMNS nanocomposites exhibited promising semiconducting properties, making them suitable for future applications in sensors, supercapacitors and electrochemical devices. Further optimization and long-term performance studies could pave the way for their practical utility in the advanced technologies.

ACKNOWLEDGEMENTS

The authors express their gratitude to Department of Chemistry, National University of Uzbekistan for their help in carrying out this work.

CONFLICT OF INTEREST

The authors declare that there is no conflict of interests regarding the publication of this article.

REFERENCES

1. X.-C. Dai, S. Hou, M.-H. Huang, Y.-B. Li, T. Li and F.-X. Xiao, *J. Phys. Energy*, **1**, 022002 (2019); https://doi.org/10.1088/2515-7655/ab2677
2. C. Yu, W. Zhang, S. Guo, B. Hu, Z. Zheng, J. Ye, S. Zhang and J. Zhu, *Nano Energy*, **66**, 104135 (2019); https://doi.org/10.1016/j.nanoen.2019.104135
3. K. Wang, G. Liu, N. Hoivik, E. Johannessen and H. Jakobsen, *Chem. Soc. Rev.*, **43**, 1476 (2014); https://doi.org/10.1039/C3CS60150A
4. C. Li, Y. Ni, J. Gong, Y. Song, T. Gong and X. Zhu, *Nanoscale Adv.*, **4**, 322 (2022); https://doi.org/10.1039/D1NA00624J
5. K. Lee, A. Mazare and P. Schmuki, *Chem. Rev.*, **114**, 9385 (2014); https://doi.org/10.1021/cr500061m
6. A.M. El-Khawaga, A. Zidan and A.I.A.A. El-Mageed, *J. Mol. Struct.*, **1281**, 135148 (2023); https://doi.org/10.1016/j.molstruc.2023.135148
7. J.S. Santos, P.D.S. Araujo, Y.B. Pissolitto, P.P. Lopes, A.P. Simon, M.D.S. Sikora and F. Trivinho-Strixino, *Materials*, **14**, 383 (2021); https://doi.org/10.3390/ma14020383
8. Y. Xu and G. Zangari, *Coatings*, **11**, 931 (2021); https://doi.org/10.3390/coatings11080931
9. S.A. Batool, M. Salman Maqbool, M.A. Javed, A. Niaz and M.A.U. Rehman, *Surfaces*, **5**, 456 (2022); https://doi.org/10.3390/surfaces5040033
10. X. Sun, X. Mo, L. Liu, H. Sun and C. Pan, *ACS Appl. Mater. Interfaces*, **11**, 21661 (2019); https://doi.org/10.1021/acsami.9b02593
11. L. Mohan, C. Dennis, N. Padmapriya, C. Anandan and N. Rajendran, *Mater. Today Commun.*, **23**, 101103 (2020); https://doi.org/10.1016/j.mtcomm.2020.101103
12. K. Zhang, S. Cao, C. Li, J. Qi, L. Jiang, J. Zhang and X. Zhu, *Electrochem. Commun.*, **103**, 88 (2019); https://doi.org/10.1016/j.elecom.2019.05.015
13. M. Zhang and J. Li, *Mater. Today*, **12**, 12 (2009); https://doi.org/10.1016/S1369-7021(09)70176-2
14. J.H. Lehman, M. Terrones, E. Mansfield, K.E. Hurst and V. Meunier, *Carbon*, **49**, 2581 (2011); https://doi.org/10.1016/j.carbon.2011.03.028
15. R. Zhang, Y. Zhang and F. Wei, *Chem. Soc. Rev.*, **46**, 3661 (2017); https://doi.org/10.1039/C7CS00104E
16. N. Bashirom, K.A. Razak, C.K. Yew and Z. Lockman, *Procedia Chem.*, **19**, 611 (2016); https://doi.org/10.1016/j.proche.2016.03.060
17. K.S. Raja, T. Gandhi and M. Misra, *Electrochem. Commun.*, **9**, 1069 (2007); https://doi.org/10.1016/j.elecom.2006.12.024
18. H. Zhang, Z. Chen, Y. Song, M. Yin, D. Li, X. Zhu, X. Chen, P.C. Chang and L. Lu, *Electrochem. Commun.*, **68**, 23 (2016); https://doi.org/10.1016/j.elecom.2016.04.004
19. Y. Zhang, W. Cheng, F. Du, S. Zhang, W. Ma, D. Li, Y. Song and X. Zhu, *Electrochim. Acta*, **180**, 147 (2015); https://doi.org/10.1016/j.electacta.2015.08.098
20. J.R. González, R. Alcántara, F. Nacimiento, G.F. Ortiz, J.L. Tirado, E. Zhecheva and R. Stoyanova, *J. Phys. Chem. C*, **116**, 20182 (2012); https://doi.org/10.1021/jp3050115
21. Y. Zhang, W. Cheng, F. Du, S. Zhang, W. Ma, D. Li, Y. Song and X. Zhu, *IOP Conf. Series: Mater. Sci. Eng.*, **116**, 012025 (2015); https://doi.org/10.1016/j.electacta.2015.08.098
22. Z. Chamanzadeh, M. Noormohammadi and M. Zahedifar, *Mater. Res. Express*, **5**, 055025 (2018); https://doi.org/10.1088/2053-1591/aac1f5
23. Y. Cheng, Z. Peng, X. Wu, J. Cao, P. Skeldon and G.E. Thompson, *Electrochim. Acta*, **165**, 301 (2015); https://doi.org/10.1016/j.electacta.2015.03.020
24. E. Montakhab, F. Rashchi and S. Sheibani, *Appl. Surf. Sci.*, **534**, 147581 (2020); https://doi.org/10.1016/j.apsusc.2020.147581
25. S. Farsinezhad, Ph.D. Thesis, TiO_2 Nanotube Arrays with Engineered Geometries: Growth, Characterization and Study of Selected Interfaces, Department of Electrical and Computer Engineering Faculty of Engineering, University of Alberta, Edmonton, Canada (2016).
26. P. Junbang, C. Aiempanakit and K. Aiempanakit, *J. Metals, Mater. Miner.*, **32**, 24 (2022); https://doi.org/10.55713/jmmm.v32i2.1256
27. H.P. Quiroz, F. Quintero, P.J. Arias, A. Dussan and H.R. Zea, *J. Phys. Conf. Ser.*, **614**, 012001 (2015); https://doi.org/10.1088/1742-6596/614/1/012001
28. A. Robin, M.B. de Almeida Ribeiro, J.L. Rosa, R.Z. Nakazato and M.B. Silva, *J. Surf. Eng. Mater. Adv. Technol.*, **4**, 123 (2014); http://dx.doi.org/10.4236/jsemat.2014.43016
29. I.C. Turu and N. Cansever, *Int. J. Electrochem. Sci.*, **17**, 220624 (2022); https://doi.org/10.20964/2022.06.33
30. Aamina, M.A. Hossen and A. Abd Aziz, *Construction*, **3**, 230 (2023); https://doi.org/10.15282/construction.v3i2.9773
31. Z. Endut, Ph.D. Thesis, Synthesis and Characterization of Anodic Titania Nanotubes for Supercapacitor Application, University of Malaya (Malaysia) (2013).
32. Z. Zhang, Q. Liu, M. He, F. Tang, Z. Ying, H. Xu, Y. Song, J. Zhu, and X. Zhu, *J. Electrochem. Soc.*, **167**, 113501 (2020); https://doi.org/10.1149/1945-7111/aba00b
33. A. Acquesta, A. Carangelo and T. Monetta, *Metals*, **8**, 489 (2018); https://doi.org/10.3390/met8070489
34. Y.H. Li, S. Wang, X. Zhang, J. Wei, C. Xu, Z. Luan and D. Wu, *Mater. Res. Bull.*, **38**, 469 (2003); https://doi.org/10.1016/S0025-5408(02)01063-2
35. O.R. Aguirre and E.F. Echeverría, *Appl. Surf. Sci.*, **445**, 308 (2018); https://doi.org/10.1016/j.apsusc.2018.03.139
36. M. Beygisangchin, S.A. Rashid, H.N. Lim, S. Shafie and A.R. Sadrolhosseini, *Opt. Mater.*, **131**, 112711 (2022); https://doi.org/10.1016/j.optmat.2022.112711
37. H.M. Yusop and W.W. Ismail, *Malaysian J. Chem.*, **23**, 40 (2021).
38. M.A. White, Physical Properties of Materials. CRC Press, Boca Raton (2018).
39. V. Stone, B. Nowack, A. Baun, N. van den Brink, F. von der Kammer, M. Dusinska, R. Handy, S. Hankin, M. Hassellöv, E. Joner and T.F. Fernandes, *Sci. Total Environ.*, **408**, 1745 (2010); https://doi.org/10.1016/j.scitotenv.2009.10.035
40. C. Nieto-Draghi, G. Fayet, B. Creton, X. Rozanska, P. Rotureau, J.C. de Hemptinne, P. Ungerer, B. Rousseau and C. Adamo, *Chem. Rev.*, **115**, 13093 (2015); https://doi.org/10.1021/acs.chemrev.5b00215
41. M.J. Frisch, G.W. Trucks, H.B. Schlegel, G.E. Scuseria, M.A. Robb, J.R. Cheeseman, G. Scalmani, V. Barone, B. Mennucci, G.A. Petersson, H. Nakatsuji, M. Caricato, X. Li, H.P. Hratchian, A.F. Izmaylov, J. Bloino, G. Zheng, J.L. Sonnenberg, M. Hada, M. Ehara, K. Toyota, R. Fukuda, J. Hasegawa, M. Ishida, T. Nakajima, Y. Honda, O. Kitao, H. Nakai, T. Vreven Jr., J.A. Montgomery, J.E. Peralta, F.M. Ogliaro, J. Bearpark, J. Heyd, E. Brothers, K.N. Kudin, V.N. Staroverov, R. Kobayashi, J. Normand, K. Raghavachari, A. Rendell, J.C. Burant, S.S. Iyengar, J. Tomasi, M. Cossi, N. Rega, J.M. Millam, M. Klene, O. Yazyev, A.J. Austin, R. Cammi, C. Pomelli, J.W. Ochterski, R.L. Martin, K. Morokuma, V.G. Zakrzewski, G.A.P. Salvador, S. Dapprich, J.J. Dannenberg, A.D. Daniels, O. Farkas, J.B. Foresman, J.V. Ortiz and J. Cioslowski, D.J. Fox, Gaussian 09, Revision D.01, Gaussian, Inc., CT Wallingford (2009).